Analyst

PAPER

Cite this: *Analyst*, 2016, **141**, 1363

Nanomaterial size distribution analysis *via* liquid nebulization coupled with ion mobility spectrometry (LN-IMS)†

Seongho Jeon,[a] Derek R. Oberreit,[b] Gary Van Schooneveld[c] and Christopher J. Hogan Jr.*[a]

Received 18th October 2015,
Accepted 29th December 2015

DOI: 10.1039/c5an02150b

www.rsc.org/analyst

We apply liquid nebulization (LN) in series with ion mobility spectrometry (IMS, using a differential mobility analyzer coupled to a condensation particle counter) to measure the size distribution functions (the number concentration per unit log diameter) of gold nanospheres in the 5–30 nm range, 70 nm × 11.7 nm gold nanorods, and albumin proteins originally in aqueous suspensions. In prior studies, IMS measurements have only been carried out for colloidal nanoparticles in this size range using electrosprays for aerosolization, as traditional nebulizers produce supermicrometer droplets which leave residue particles from non-volatile species. Residue particles mask the size distribution of the particles of interest. Uniquely, the LN employed in this study uses both online dilution (with dilution factors of up to 10^4) with ultra-high purity water and a ball-impactor to remove droplets larger than 500 nm in diameter. This combination enables hydrosol-to-aerosol conversion preserving the size and morphology of particles, and also enables higher non-volatile residue tolerance than electrospray based aerosolization. Through LN-IMS measurements we show that the size distribution functions of narrowly distributed but similarly sized particles can be distinguished from one another, which is not possible with Nanoparticle Tracking Analysis in the sub-30 nm size range. Through comparison to electron microscopy measurements, we find that the size distribution functions inferred *via* LN-IMS measurements correspond to the particle sizes coated by surfactants, *i.e.* as they persist in colloidal suspensions. Finally, we show that the gas phase particle concentrations inferred from IMS size distribution functions are functions of only of the liquid phase particle concentration, and are independent of particle size, shape, and chemical composition. Therefore LN-IMS enables characterization of the size, yield, and polydispersity of sub-30 nm particles.

1. Introduction

Methods to efficiently determine the size, polydispersity, and concentrations of nanomaterials in liquid suspensions are extremely important in nanomanufacturing systems, particularly for nanomaterials (nanoparticles) in the sub 30 nm size range. Nanoparticles in this size range can exhibit strong size dependent optoelectronic[1,2] and catalytic[3,4] properties; extremely accurate and reliable techniques to quantify not only the mean size, but the polydispersity and yield are hence critical in liquid phase synthesis process monitoring. Unfortunately, commonly applied size analysis techniques are limited in capabilities below 30 nm. Aside from electron microscopy (which is time consuming, particularly to infer size and shape distributions with appropriate counting statistics), nanoparticles size distribution functions (the particle number concentration per unit diameter or per unit log diameter, quantifying the size, concentration, and polydispersity) are frequently determined *via* photon correlation spectroscopy/dynamic light scattering.[5–8] Because of the indirect nature of the measurement, it is difficult to apply photon correlation spectroscopy to infer the size distribution functions of highly polydisperse or multimodal samples, and inferred distributions are commonly biased towards larger particles.[9] Further, quantification of nanoparticle concentrations is often not possible. Recently developed Nanoparticle Tracking Analysis (NTA),[10–14] in which the motion of individual particles is monitored and used to infer the size distribution function, does not require the fitting procedures normally associated

[a]*Department of Mechanical Engineering, University of Minnesota, Minneapolis, MN, USA. E-mail: hogan108@ umn.edu; Fax: +1-612-625-6069; Tel: +1-612-626-8312*
[b]*Kanomax-FMT, St Paul, MN USA*
[c]*CT Associates, Inc., Eden Prairie, MN USA*

† Electronic supplementary information (ESI) available: Schematic diagrams of the LN and LN-IMS system, a description of droplet size distribution function measurements, tables listing all measurements made, and the size distribution functions of albumin proteins. See DOI: 10.1039/c5an02150b

with photon correlation spectroscopy. However, NTA is difficult to apply to particles appreciably smaller than the wavelengths of visible light, *i.e.* particles smaller than 30 nm are not easily detected. Sub 10 nm particles can often be analyzed by size exclusion chromatography,[15] but particles can clog columns, and the resolution of this technique reduces with increasing size. Finally, flow field fractionation[16] and analytical ultracentriguation[17,18] can be applied for sub 30 nm particle analysis, though both need to be coupled to appropriate detectors for particles.

Overall, the development of easy-to-apply size distribution measurement procedures remains a critical issue in nanomanufacturing, as synthesis process monitoring must be applied repeatably (*i.e.* to each "batch" of nanomaterials). Further, different size distribution measurement procedures have been found to give results in disagreement with one another in several circumstances,[9,19] with the underlying origins of disagreement still unclear. Additional comparison of the performance of existing techniques amongst one another, as well as comparison to newly developed techniques for a variety of nanomaterials, remains necessary.

In converse to the issues confronted when analyzing nanoparticles in liquids, in aerosols, nanoparticle size distribution analysis is facilitated by ion mobility spectrometry (IMS), specifically using a differential mobility analyzer[20] coupled with a condensation particle counter[21] (DMA-CPC analysis). DMA-CPC measurements require no assumptions regarding the shape or modality of the size distribution function, and when a proper inversion routine is applied,[22] this type of analysis facilitates size distribution function determination in the 2–500 nm range. Application of the DMA-CPC technique to liquid suspensions is also possible, provided that the particles of interest can be aerosolized preserving their size distribution function. Along these lines, several studies[23,24] have examined the use of pneumatic nebulization to spray nanoparticle suspensions and evaporate the solvent, leaving aerosol nanoparticles amenable to IMS. Unfortunately, traditional nebulizers produce supermicrometer droplets; such droplets typically contain high enough concentrations of non-volatile solute (even with high purity-solvents) such that aerosolization leads to a residue coating on nanoparticles and to the production nanoparticles composed entirely of previously dissolved solute. Residue coating can shift the sizes of sub-30 nm particles by several to tens of nanometers, and the size distribution function of residue nanoparticles can mask entirely the particles of interest.[25] This limits analysis to >50 nm particles in most circumstances. Additionally, multiple nanoparticles can be present within the same droplet, and these nanoparticles will agglomerate with one another upon solvent drying. As an alternative to pneumatic nebulization, Fernandez de la Mora and coworkers,[26] Kaufman and coworkers,[25,27,28] Lenggoro and coworkers,[29–31] and more recently Tsai, Zachariah & coworkers[32–39] have examined the use of electrosprays followed by charge reduction[40,41] to produce submicrometer (down to 100 nm) droplets. Electrosprays facilitate the aerosolization of aqueous particles with minimal shifts in the size distribution function. Though this technique has been successfully applied to metal nanoparticles,[30,36,42] polymers,[43–45] proteins,[27,28,46] as well as viruses and virus-like particles,[47–54] there are still drawbacks to using electrosprays for aerosolization; namely, (1) there are rather strict requirements on the electrical conductivities of suspensions which can be electrosprayed,[55,56] and (2) non-volatile solutes need to be removed from the suspension prior to electrospray based aerosolization (*i.e.* electrospray based aerosolization still leads to the formation of residue particles from solutes).[25] These requirements have limited the application electrospray-DMA based analyses to highly purified protein and virus samples. In total, because of the lack of robust aerosolization techniques, though fast and relatively inexpensive, IMS approaches have not been widely adopted for nanoparticle size distribution analysis in liquids.

In the interest of improving the utility of IMS in nanoparticle analysis, here we apply a recently developed liquid nebulizer (LN) to aerosolize nanoparticles, and subsequently show that their size distributions can be analyzed *via* IMS, *i.e.* with a DMA-CPC combination. Unique from most pneumatic nebulizers, the LN applied in this work utilizes online dilution with ultrapure water (UPW) with dilution factors (UPW flowrate/sample flow rate) in excess of 10^2, and an inertial impactor to remove large droplets prior to analysis. The dilution-impaction combination leads to minimal perturbation of the particle size distribution during aerosolization. Using the LN, we made IMS measurements of sub 30 nm gold nanospheres (down to 5 nm in nominal diameter), gold nanorods, and albumin proteins in aqueous suspensions with variable pH and concentration of phosphate buffered saline. Importantly, we show that independent of particle size, shape, and solute concentration, a calibration curve can be developed linking measured aerosol concentrations to the nanoparticle concentrations in suspension. Results are compared to electron microscopy and NTA. To our knowledge, this is the first demonstration of quantitative, IMS-based size distribution function measurement of sub-20 nm nanomaterials in which nanomaterials were aerosolized without the use of electrospray.

2. Materials and methods

2.1. Nanoparticle suspensions

Gold nanospheres of five nominal diameters (5, 7, 10, 15, and 30 nm, which had manufacturer reported mean diameter ± standard deviations of 5.06 ± 0.77 nm, 7.20 ± 0.82 nm, 12.05 ± 0.99 nm, 17.06 ± 1.70 nm, 30.02 ± 3.86 nm, respectively) as well as 980 nm resonant gold nanorods (GNRs, which were nominally 70.5 nm in length × 11.7 nm in diameter) were all purchased from Nanocomposix, Inc. (San Diego, CA, USA). To stabilize suspensions, gold nanospheres were pretreated with tannic acid and the surface of gold nanorods was coated with citrate anions (subsequent to synthesis). Bovine serum albumin (BSA, CAS registration #: 9048-46-8) and ovalbumin (OVA, albumin from chicken egg white, CAS registration #:

9006-59-1) were also examined and were purchased from Sigma Aldrich (Saint Louis, MO, USA). Suspensions were prepared with a variety of solutes and with number concentrations in the 2.00×10^9 mL^{-1} to 8.16×10^{14} mL^{-1} range. First, gold nanosphere suspensions were either used directly (with tannic acid included) in experiments or diluted offline (to vary concentrations) with UPW, which had total organic carbon and non-volatile residue levels below 1 ppbv, was treated with 165 nm UV-light and was passed 10 nm & 20 nm particle filtration systems as well as a mixed bed ion exchange resin. The pH of suspensions was controlled to be 5.0–9.7 by adding either acetic acid (BDH Aristar) or ammonium hydroxide (Macron Fine Chemicals). Second, gold nanospheres were diluted (to varying concentration levels) in 0.001×–0.01× phosphate buffered saline (PBS, Corning Life Science, CA, USA). At this PBS concentration level, gold nanospheres were found stable in suspension for more than seven days (by visual examination). GNR suspensions were found to contain significantly higher concentrations of non-volatile solutes, hence prior to measurement GNR suspensions were diluted one-hundred fold in de-ionized (DI) water (produced using a SpectraPure, Tempe, USA filtration system, and not filtered to the extent of the UPW), centrifuged twice (7600 rpm for 15 minutes with a model 5418 centrifuge, Eppendorf, Hamburg, Germany), and finally resuspended in DI water. We note that this preparation procedure is considerably simpler than that used in preparing GNRs for electrospray based aerosolization previously.[57,58] BSA and OVA samples were prepared by dissolving known weights (from which number concentrations were determined) in UPW, with the suspension pH similarly varied by addition of acetic acid and ammonium hydroxide. BSA and OVA samples were also prepared in 0.01× and 0.05× PBS.

2.2. Liquid nebulizer -ion mobility spectrometry (LN-IMS) measurements

A schematic diagram of the LN is provided in Fig. S1a,† and a schematic diagram of the LN coupled with a DMA and CPC for IMS measurements is shown in Fig. S1b, both in the ESI.† The LN (LiquiTrak® Model 7788, Fluid Measurement Technologies, Inc., St Paul, MN, USA), similar to the model employed by Fissan *et al.*,[24] was designed to have (1) a small air–liquid mixing chamber to maximize the breakup of liquid into droplets, (2) a small existing orifice diameter, generating back pressure on the sample flow and further promoting droplet formation, and (3) a ball-type inertial impactor at the exit of the nebulizer to efficiently remove larger droplets from the generated aerosol. The generated droplet size distribution function has been measured by the residue method,[56] and is reported on in the ESI (including Fig. S2,† the droplet size distribution function). Briefly, the droplet size distribution function is found to be approximately lognormal, with a geometric mean diameter of 99.8 nm and a geometric standard deviation of 2.32. For LN operation, a colloidal suspension is pumped at a flow rate in the 0.01 to 1.0 milliliter per minute (mL min^{-1}) range; this flow is mixed with UPW flowing at 100 ml min^{-1}, with combined outlet inline with the UPW inlet, and the sample flow inlet oriented perpendicular to the UPW inlet and combined outlet. The ratio of these two flow rates defines a dilution factor (DF) for the sample, which can be varied from 10^2 to 10^4. After mixing, ~98 mL min^{-1} of the flow is diverted to a waste stream, while 2 mL min^{-1} is directed into a single nozzle, where it is mixed with 0.6 standard L min^{-1} of air at 19 °C (monitored continuously during measurement). Upon exiting the nebulizer, an evaporator (at 57–60 °C) facilitates solvent volatilization, leaving a flowing aerosol composed of particles and non-volatile solutes originally in the liquid sample.

For IMS measurements, 1.5 l min^{-1} of the nebulized particle flow is introduced into a soft X-ray ionization chamber (Advanced Aerosol Neutralizer 3087, TSI Inc., Shoreview, MN, USA).[59] Soft X-ray irradiation generates roughly equal concentrations of positive and negative ions from trace organic molecules (at part-per-trillion levels) in air (photoionization);[60,61] these ions subsequently collide with particles and transfer charge to them upon collision. After remaining in the ionization chamber for a sufficient amount of time, the particles achieve known size-dependent charge distribution function, wherein most particles are neutral and the majority of charged particles are singly charged.[62,63] Particles are then directed into a DMA (model 3085, TSI Inc.);[64] DMAs act as narrow band mobility filters, only transmitting particles in a mobility range governed by their sheath flowrate (15 l min^{-1}) and the applied potential difference between electrodes. Particles transmitted through the DMA are detected by a CPC (model 3776, TSI Inc.). The DMA and CPC are operated in tandem as a scanning mobility particle spectrometer (SMPS)[65] with 120 second upward voltage scans applied, 15 second downscans, and ~60 seconds between scans.

The LN-IMS measurements reported here were performed as follows. First, the gold nanospheres, GNRs, and the two proteins were nebulized separately and examined at variable analyte concentrations and dilution ratios, as well as variable PBS concentration and pH. Subsequently, six mixtures, each composed of two different sized sub-30 nm gold nanospheres were measured. Tables listing each sample analyzed, its initial number concentration, pH, PBS concentration, and online dilution factor is provided in the ESI.†

2.3. Nanosight™ and transmission electron microscope

LN-IMS measurements were compared to NTA measurements made with a Nanosight™ LM-14 (Malvern Instruments LTD, Malvern, Worcestershire, UK), as well as transmission electron microscopy (TEM, FEI, Hillsboro, OR, USA) measurements. With NTA, we examined the size distributions of both monodisperse (10, 15, 30, and 60 nm in diameter) and polydisperse (15 & 30 nm, and 30 & 60 nm, mixtures) gold nanospheres. Because the recommended particle concentration for NTA measurements is $<10^9$ particles per mL, the original gold nanosuspensions were diluted with DI water (SpectraPure, Tempe, USA) by a factor of 10^2–10^3. At least 5 measurements were performed for each sample and the hydrodynamic size distribution function was inferred using the procedure

described by Jeon *et al.*,[66] in lieu of using the Nanosight™ software program. For TEM measurements, an FEI Tecnai T12 TEM (in the University of Minnesota Characterization Facility) was used to image the gold nanospheres and the GNRs. 10–30 μl of each analyte suspension were dropped onto a carbon grid (200 mesh, Ted Pella INC, CA, USA) and the solvent was allowed to evaporate. The software 'ImageJ' was employed to measure particle sizes in TEM images. More than 300 individual particles were examined for each sample to establish an accurate particle size distribution. The TEM was calibrated monthly and measurements are expected to be accurate to within 0.1 nm. For the GNRs, the measurement of the width and length of each rod enabled the inference of its hydrodynamic radius (R_H) and projected area (PA), which enabled direct comparison to LN-IMS measurements.[57]

3. Results & discussion

3.1. Size distribution Functions

Size distribution function measurements involve inversion of the function $\frac{dn}{d\log_{10}(d_p)}$, the number concentration per unit $\log_{10}$ of particle diameter (d_p). In LN-IMS mesaurements, this distribution is determined not in the liquid phase, but the gas phase, *via* measurement of particle number concentrations (n_i) with a DMA operated under voltage settings "i". n_i and $\frac{dn}{d\log_{10}(d_p)}$ are linked *via* the equation:

$$n_i = \sum_{z=+1}^{z=+\infty} \int_{-\infty}^{\infty} \eta_{CPC}(d_p)\theta_i(d_p,z)\eta_D(d_p)f_z(d_p,z)\frac{dn}{d\log_{10}(d_p)}d\log_{10}(d_p) \quad (1a)$$

where $\eta_{CPC}(d_p)$ is size dependent detection efficiency of the CPC, $\theta_i(d_p,z)$ is the DMA tansfer function under settings "i" (with settings corresponding to sheath flowrate, aerosol inlet and outlet flowrates, and applied voltage), $\eta_D(d_p)$ is the size dependent fraction of particles transmitted through the DMA-CPC system (*i.e.* those that did not diffusionally deposit), and $f_z(d_p,z)$ is the fraction of particles of integer charge state z exiting the soft X-ray photoionizer. To determine $\frac{dn}{d\log_{10}(d_p)}$, measurements must be made at a sufficient number of settings "i", an inversion routine must be applied to solve eqn (1a), and all functions except n_i (the observable) must be known *a priori*. We applied the built-in SMPS software and DMA transfer function available with TSI instruments for inversion (Aerosol Instrument Manager), in which the CPC detection efficiency in the size range of interest was unity, the Stokes-Millikan equation[67,68] was used to link the mobility to the particle diameter, transmission efficiencies were calcuated using the Gormely-Kennedy equations,[69] and $f_z(d_p, z)$ was calculated *via* the regression equations of Wiedensohler[63] (which recent studies suggest are reasonably valid for spheres and nanorods[62,70]). None of these functions are strongly dependent on the chemical nature of the particles examined. We thus postulate that when plotted against the analyte suspension concentration, the dilution corrected number concentration of particles (n_{tot}), described by the equation:

$$n_{tot} = DF\int_{-\infty}^{\infty}\frac{dn}{d\log_{10}(d_p)}d\log_{10}(d_p) \quad (1b)$$

should collapse to an analyte (size, shape, and chemical composition) and solute independent function. In the remaining sub-sections, we (1) report the inverted size distribution functions from LN-IMS for all samples, (2) examine (numerically) the LN conditions required to preserve size distribution functions during aerosolization, (3) compare LN-IMS measurements to NTA and TEM analysis, and (4) demonstrate that the dilution factor corrected aerosol number concentration is in fact solely dependent on the original suspension number concentration.

3.2. LN-IMS size distribution functions

The size distribution functions (averaged over 10 consecutive scans) of 5, 7, 10, 15 and 30 nm diameter gold nanospheres and GNRs, nebulized at a pH near 7, are shown in Fig. 1. Best fit lognormal distribution functions are also displayed on these plots, with the geometric mean diameter (d_{pg}) and geometric standard deviation (σ_g) are also noted on the figure. For all examined particles, σ_g values were below 1.2, indicating that narrowly distributed particles were detected. Similar plots for BSA and OVA are shown in the ESI (Fig. S3†), where we obtained mode diameters of 6.4 nm and 5.7 nm, respectively. These protein effective diameters are in good agreement with higher resolution IMS measurements of low charge state BSA and OVA collision cross sections.[71–73] We additionally found the geometric mean diameter and standard deviation to be independent of DF, provided that DF was sufficiently high to reduce the sizes of residue particles well below the sizes of the particles and to mitigate droplet induced aggregation. While in total these results suggest that LN-IMS measurements enable accurate size distribution function inference, for the gold nanospheres, all d_{pg} values were slightly larger than the nominal diameters and manufacturer reported mean diameters for several samples; we remark further on this observation in comparison to TEM measurements in section 3.4.

The non-volatile residue present in the samples examined in Fig. 1 derives from surfactants used in stabilizing nanoparticles in suspension as well as salts used during particle synthesis. Of interest is also examination influence additional solutes may have on LN-IMS measurements, as well as changes in pH. Fig. 2 displays the size distribution functions of 10 nm and 15 nm gold nanospheres from DI water (with non-volatile residue remaining from their original suspension), 0.005× PBS, and in pH 9.7 suspensions. The initial suspension concentration and dilution factor are labelled for each measurement. Similar results were obtained for gold nanospheres of other sizes, and both protein samples. Evident by comparison of the Fig. 2 plots to one another is that the peak

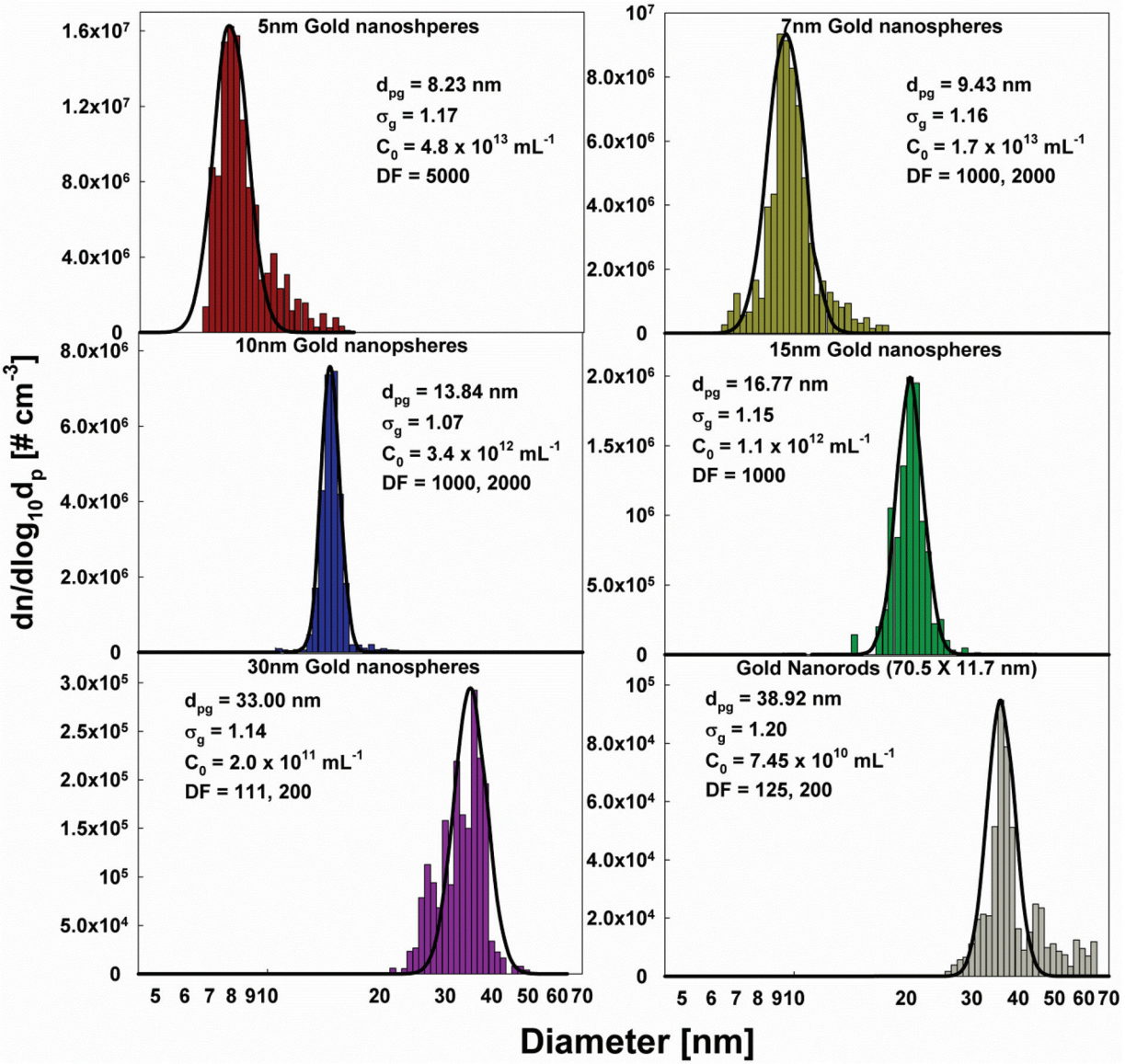

Fig. 1 LN-IMS inferred size distribution functions for gold nanospheres and GNRs.

diameter of the distribution functions corresponding to gold nanospheres do not shift from DI water to PBS or pH = 9.7 suspensions. Further, we did not observe any changes to size distribution functions over time, suggesting that gold nanoparticles did not aggregate in any of the test suspensions. However, also visible in distribution functions are residue particles at separate, smaller diameter, modes in both the PBS and pH = 9.7 size distribution functions; such peaks arise because (1) these suspensions were of lower concentration than the original and lower dilution factors were used, and (2) the concentrations of non-volatile solutes were higher in these suspensions. Nonetheless, these results show that it is possible to identify and measure the size distribution functions of sub 30 nm particles *via* LN-IMS in suspensions with non-volatile residue present (which is not possible with electrospray based ionization[25]).

The size distribution functions of six gold nanosphere mixtures (7 & 15 nm, 5 & 10 nm, 15 & 30 nm, 7 & 10 nm, 7 & 30 nm and 10 & 30 nm in diameter) were examined also examined and are plotted in Fig. 3. The concentration ratios in suspension as well as the dilution factors utilized in measurements are noted. In all instances, we were able to clearly identify both particle types in mixtures. These results are compared to NTA measurements in section 3.4.

3.3. Simulation of hydrosol to aerosol conversion

The results presented in the previous section demonstrate that the LN-IMS approach is applicable to size distribution function analysis of sub 30 nm particles when appropriate dilution factors are employed. However, it does not make clear how to select such dilution factors. In this section, we present a simulation method, based upon prior simulation efforts[74–77] to

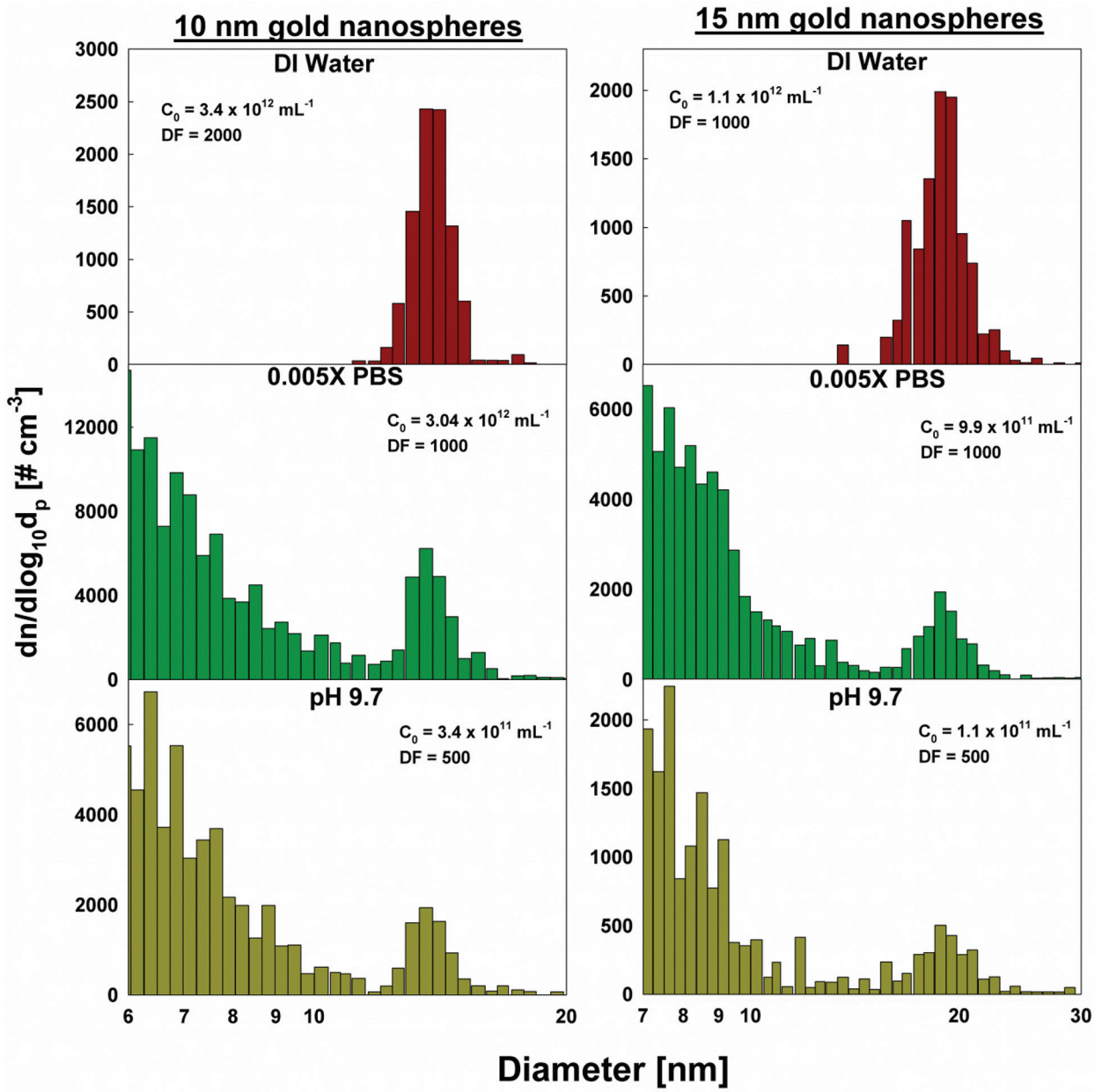

Fig. 2 LN-IMS inferred size distribution functions for nominal 10 nm and 15 nm gold nanospheres in DI water (upper), 0.005× PBS (middle), and a pH 9.7 suspension.

predict the LN-IMS inferred size distribution function. In simulations, first, we sample a droplet diameter from an input droplet size distribution function. Second, we compute the average number of analyte particles in the droplet based upon the suspension concentration and dilution factor, and use this average to sample the number of analyte particles in the droplet from a Poisson distribution. Third, the diameters for each particle in the droplet are sampled from an input particle size distribution function. Finally, the solid volume and solid diameter (after solvent evaporation) are determined based upon the total analyte particle volume present in the droplet as well as the volume of non-volatile residue (which is also an input). This sampling procedure is repeated for 10^6 droplets and a hypothetical size distribution function is then reconstructed for a given input particle size distribution function, non-volatile solute volume fraction, dilution factor, and droplet size distribution function. When an appropriate droplet size distribution function (determined by the nebulizer operating conditions) and dilution factor are chosen, the size distribution function recovered from the simulation should be faithful to the input function. As a case study, we examine the aerosolization of nominally 15 nm gold nanospheres as well as a mixture of nominally 15 & 30 nm gold nanospheres, with the normalized size distribution functions (based on TEM

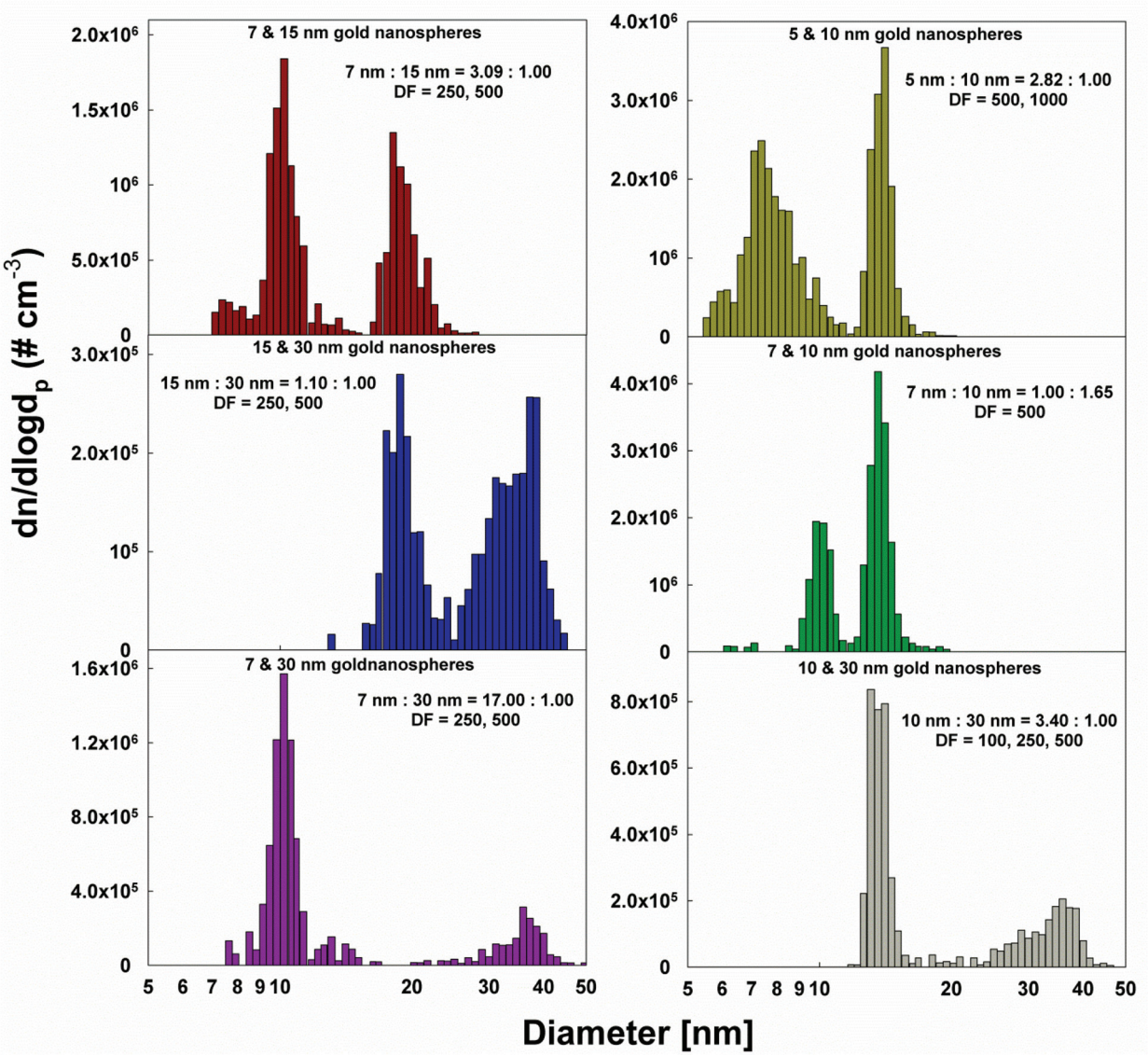

Fig. 3 LN-IMS inferred size distribution functions for gold nanosphere mixtures.

measurements) shown in Fig. 4a and b, respectively. We assumed a suspension concentration $C_0 = 10^{14}$ mL^{-1} for the 15 nm spheres and $C_0 = 2 \times 10^{14}$ mL^{-1} for the mixture, respectively. A non-volatile solute concentration of 13.7 mM NaCl (equivalent to 0.1× PBS) was also assumed. With the droplet size distribution function modeled as a Gaussian distribution with a mean of 184 nm and standard deviation 140 nm (values based on the measurements reported in Fig. S2†), the expected LN-IMS size distribution functions (normalized by the maximum value in all cases) are shown for varying dilution factors in Fig. 4c and d, respectively. At low dilution factors, for both cases a small residue peak is present (below 10 nm), and the peaks corresponding to gold nanospheres are distorted by both the formation of dimers and the presence of non-volatile residue. However, increases in the dilution factor shift the residue peak to smaller sizes and further reduce the impact of residue and aggregation on the gold nanosphere peaks; under these conditions we expect LN-IMS measurement to enable accurate inference of the colloid particle size distribution function. For comparison, in Fig. 4e and f we plot the expected size distribution functions from a nebulizer producing Gaussian distributed droplets with a mean diameter of 2.5 μm and a standard deviation of 0.7 μm (expected for traditional nebulizers). Under all conditions but DF = 10^4, the expected size distribution function does not have a peak or peaks corresponding to gold nanospheres, and with DF = 10^4, the size distribution function is still distorted by residue. This highlights clearly the need to use a nebulization scheme with small droplets to minimize the volume of non-volatile residue per droplet.

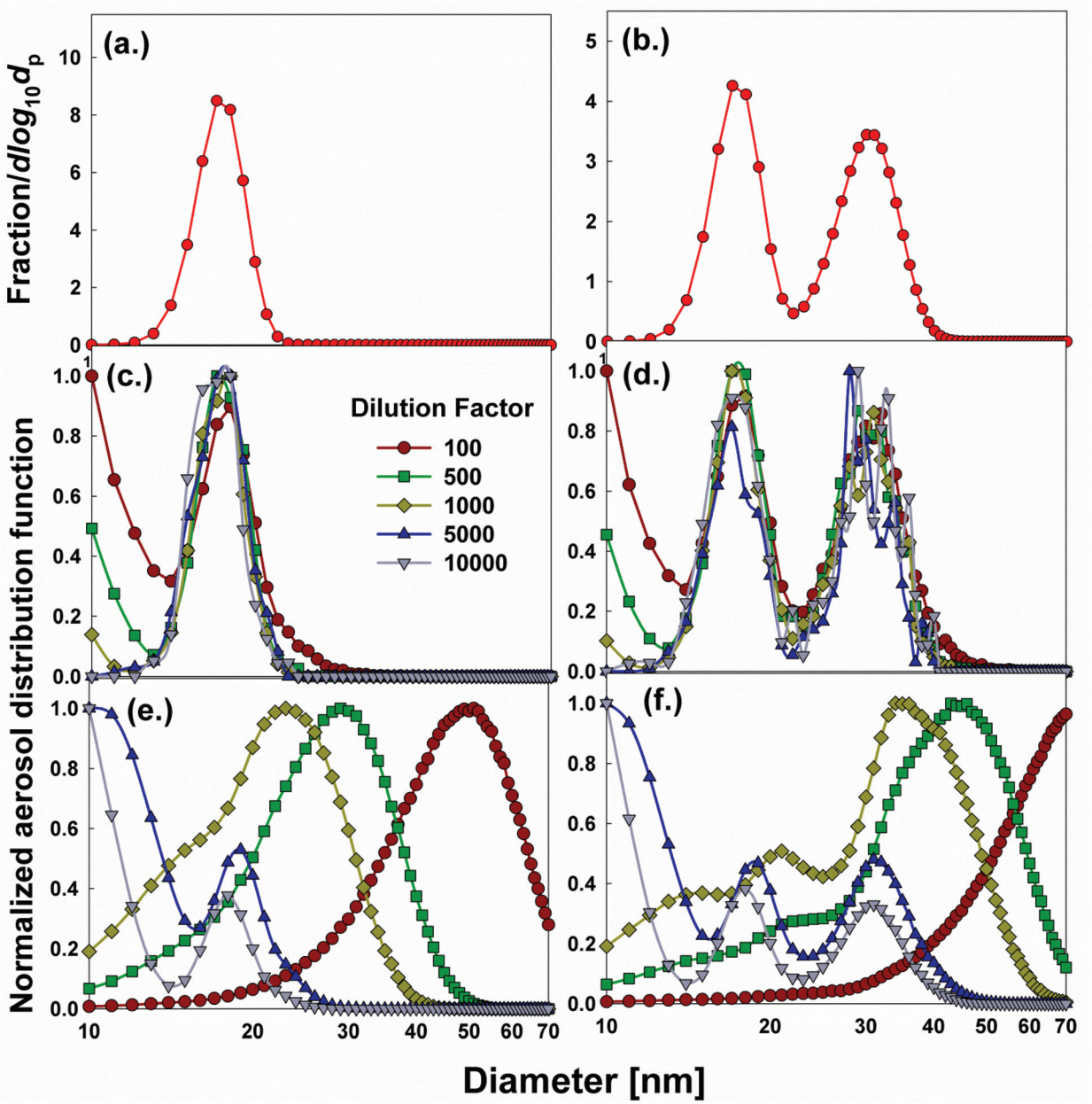

Fig. 4 The input size distribution function for (a) nominal 15 nm gold nanospheres and (b) a mixture of nominal 15 nm and 30 nm gold nanospheres. The expected LN-IMS size distribution functions (normalized by the maximum value in the 10–70 nm range) corresponding to (a) and (b) are shown in (c) and (d), respectively. The expected IMS size distributions with Gaussian distributed droplets (mean 2.5 μm, standard deviation 0.7 μm) are shown in (e) and (f).

3.4. Comparison to NTA and TEM analysis

To compare LN-IMS results to NTA measurements, we elected to examine three monodisperse samples and one mixture. NTA results are summarized in Fig. 5, with the 15 nm and 30 nm gold nanosphere mixture with the same concentration ratio as the mixture in Fig. 3. A number of issues arise when using NTA; first, the 10 nm gold nanospheres are not detected efficiently, and the mode in the distribution function appears at 30 nm. Second, though 15 nm and 30 nm particles have mode diameters near their expected values, the distributions are noticeably polydisperse, in contrast with narrow distributions inferred from LN-IMS measurements. Confirmation of the accuracy of LN-IMS measurements in determining polydispersity, as compared to NTA, is provided in Fig. 6, which displays plots of the size distribution functions for gold nanospheres and GNRs based upon TEM analysis. Size distribution functions were reconstructed by binning results and are directly comparable to Fig. 1. For the GNRs, we used the equations tested by Gopalakrishnan *et al.*[57] to estimate the

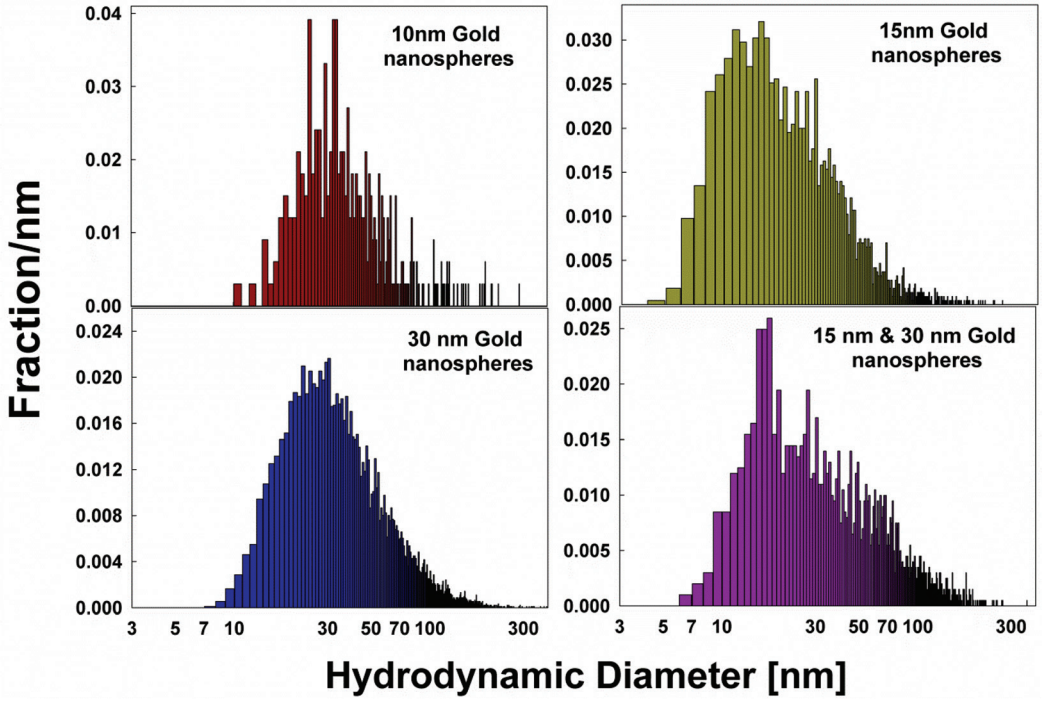

Fig. 5 A summary of the normalized size distribution functions resulting from NTA of gold nanosphere suspensions.

GNR mobility diameter (as inferred from DMA measurements) from their lengths and diameters. The geometric standard deviations inferred from LN-IMS are in good agreement with those inferred from TEM measurements; with the exception of the GNRs, the geometric standard deviations differ by 0.06 or less between the two measurements. Overall, this comparison suggests that size distribution functions inferred from NTA in the sub-30 nm size range are not necessarily accurate, with overestimation of the geometric standard and width of the distribution likely. Corroboration of this result is found in the recent work of Dudkiewicz *et al.*,[19] who examined the size distribution functions of silica nanoparticles below 250 nm by IMS (with electrospray based aerosolization), NTA, electron microscopy, centrifugal liquid sedimentation, and asymetric flow field fractionation, and found that NTA inferred size distributions had both larger means and higher polydispersities than the distributions inferred from other techniques, including IMS.

Mobility diameters, inferred by DMAs, are typically ~0.3 nm larger than the physical diameter of spherical particles, due to influence of gas molecule size on drag in the gas phase.[67] However, there are differences larger than this amount in the geometric mean diameter inferred from LN-IMS and TEM measurements in this work. For gold nanospheres, we find that the TEM geometric mean diameters are always within 0.5 nm of the nominal diameter, while the LN-IMS geometric mean diameters are 3–4 nanometers larger than the nominal diameter. A disparity of ~8 nm in effective diameter is seen for the GNRs between the two measurements. There are two possibilities for this difference which must be considered. First, the mobility diameter is inferred from the mobility based on the assumed validity of the Stokes-Millikan equation. This equation is verified primarily through measurement of organic ions[78,79] and there is some evidence that minor deviations arise for metal particles in air.[80] However, these deviations would lead to only an increase in the inferred diameter of several percent, and cannot explain the differences in inferred diameters here. We find a second possibility more plausible; differences in geometric mean diameters arise because of an organic surfactantcoating on particles (tannic acid for gold nanospheres and sodium citrate for GNRs, both of which are present on particles in suspension, serving to stabilize them against aggregation). These surfactants are sufficiently volatile to evaporate during TEM measurement (during pump down or in the electron beam) but would persist in the gas phase, increasing particle diameter. Support for this result is found in Hinterwirth *et al.*,[9] who found that for gold nanospheres in the 10–30 nm size range introduced into the gas phase *via* electrospray, the mean IMS-inferred diameters were 3–4 nm larger than those inferred from TEM. Additionally, in several prior electrospray based aerosolization studies, it was necessary to apply heating to remove surfactant coating from metal nanoparticles and without heat treatment nanoparticle size distribution functions were shifted to larger sizes by an excess of ten nanometers.[30,57] We therefore suggest that LN-IMS enables measurement of the diameters of nanoparticles including any coating bound in suspension, hence it provides information in addition to, not in-lieu of TEM

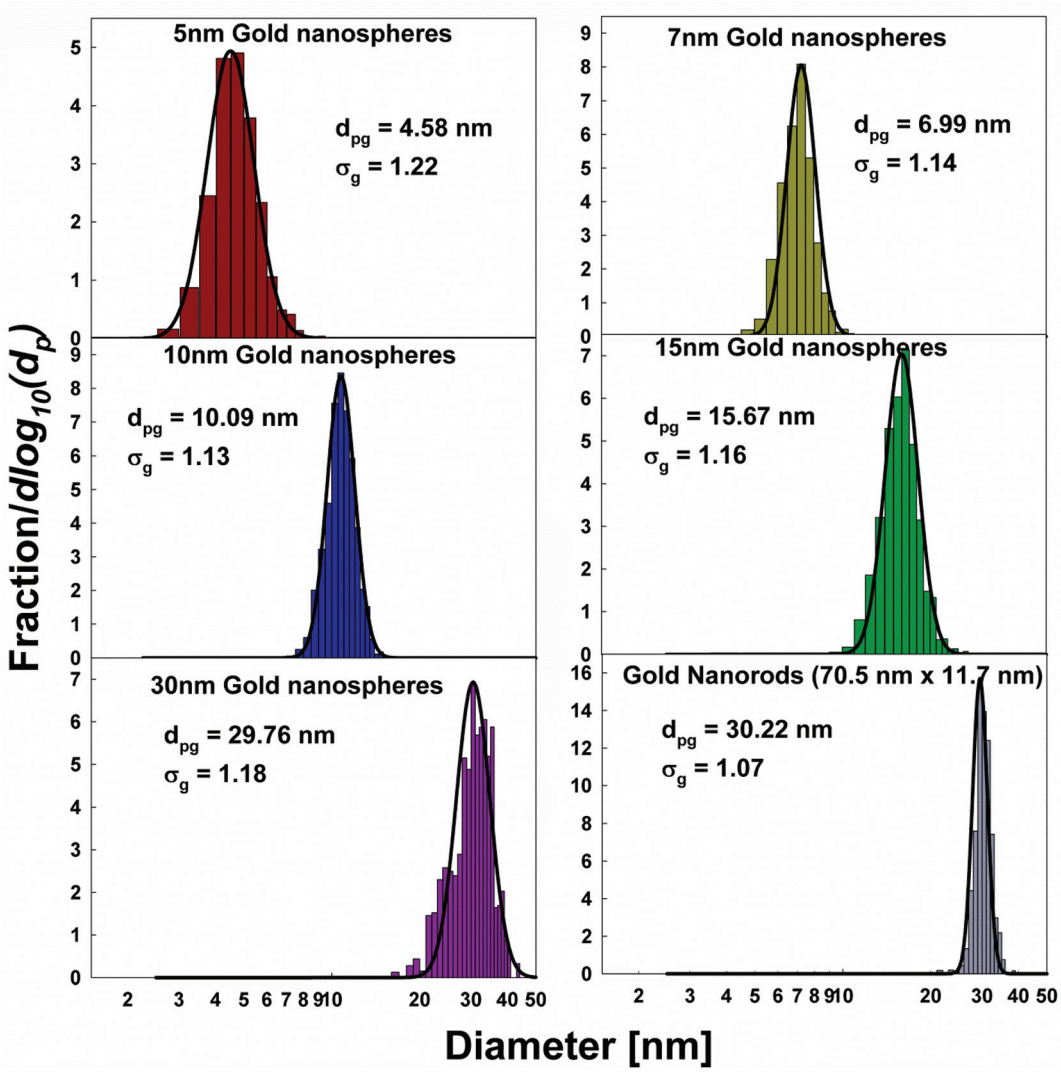

Fig. 6 TEM inferred size distribution functions for gold nanospheres and GNRs.

measurements. Further characterization of the system will be necessary to examine to what exact surfactant coating can desorb during aerosolization, and to develop methods to promote surfactant desorption.

3.5. Universal calibration curve

As remarked upon in section 3.1, total particle number concentrations integrated from size distribution functions should correlate directly with the particle concentrations in suspension; independent of particle size, shape or chemical composition. Considering all samples, the eqn (1b) inferred number concentrations are plotted *versus* suspension concentration in Fig. 7a and b. The results are separated in these two figures because the LN system was disassembled and cleaned near the midpoint of this study (which spanned more than six months). During reassembly, the position of the ball-impactor changed slightly, changing the output particle size distribution function (which ultimately influences the calibration curve linking gas phase concentration to concentration in suspension). In spite of the change caused by reassembly, apparent in both Fig. 7a and b is that the obtained gas phase concentration *versus* suspension concentration relationship does not depend upon particle size or chemical composition (*i.e.* proteins and gold nanospheres show similar results). For each set of results, a fit power law is displayed. For both plots the scaling exponent is found to be below unity; such exponents arise because at higher concentrations, there are proportionally more particles enclosed within large droplets, which are removed by the ball impactor. The differences in exponent and pre-exponential factor also arise because of changes in impactor position. Following cleaning, the exponent and pre exponential factor can be calibrated using a colloid sample standard with a known volume concentration.

While we do not observe any size dependency for the gas phase concentration *versus* liquid phase concentration relationship, there is noticeable scatter in the LN-IMS inferred

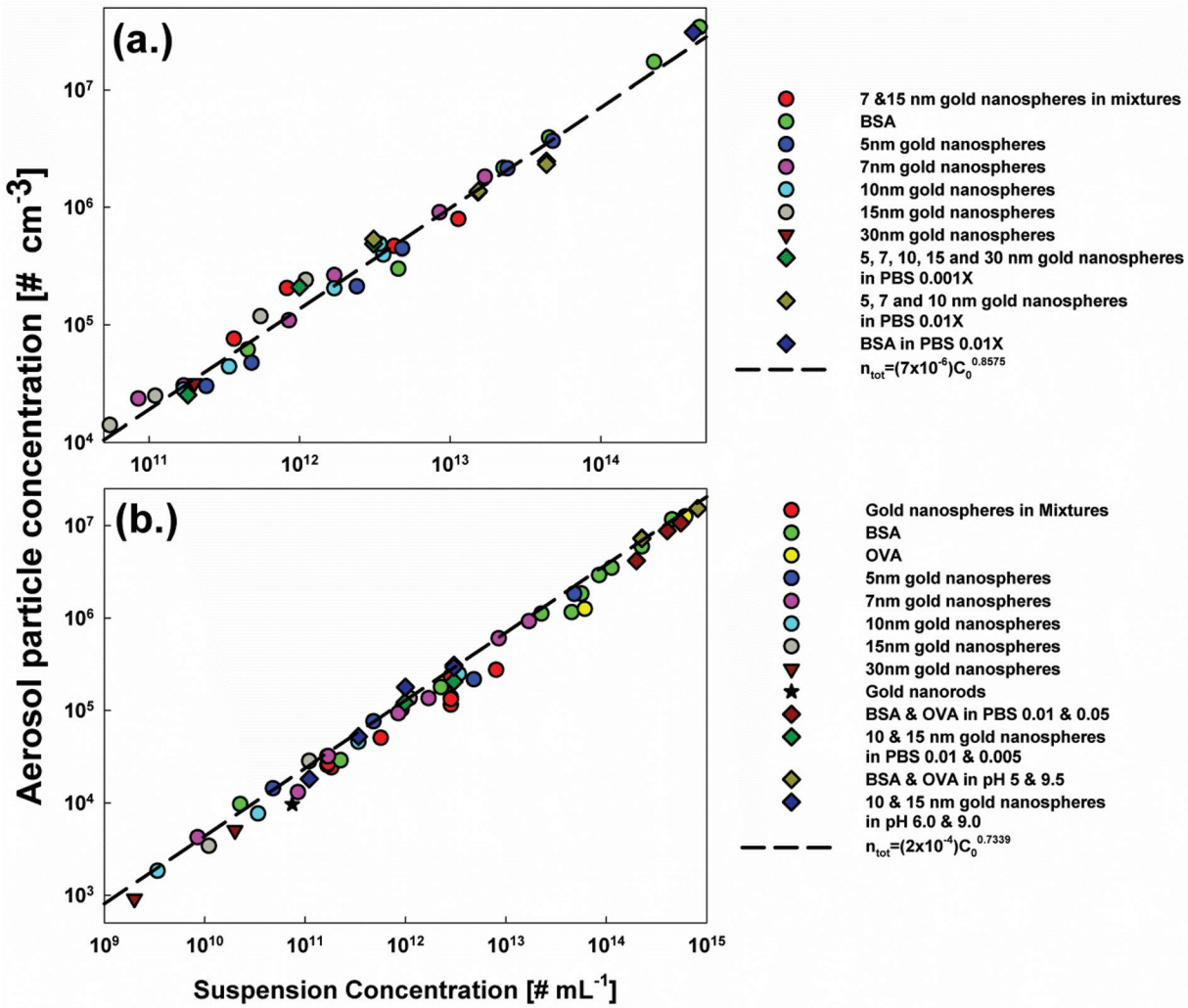

Fig. 7 Plots of the gas phase particle number concentration as a function of the original suspension concentration: (a) before disassembly and cleaning, (b) after reassembly and impactor repositioning.

number concentrations. Therefore, while it appears a universal calibration curve can be developed using a single type of nanoparticle (*e.g.* nominally 30 nm gold can be used as a standard for all particles and proteins, and can be used for polydisperse samples), suspension number concentration estimates *via* LN-IMS are only accurate to within ±20%. In many instances, this level of accuracy is sufficient; however, applications such as instrument calibration[81] may require greater level of accuracies; further refinement of size distribution inversion techniques with LN-IMS will be necessary for improved accuracy.

4. Conclusions

We have applied an LN-IMS measurement system for the measurement of gold nanosphere and nanorod as well as albumin protein size distribution function measurement. Through both experimental measurements and modeling, we show that it is possible to convert hydrosols to aerosols while minimally disturbing the particle size distribution functions. Through comparison to TEM measurements, we show that LN-IMS measurements enable accurate inference of particle polydispersity, but that the size distribution function is shifted by surfactant coating which is not observed in TEM. Importantly, we demonstrate that the gas phase particle number concentration is a size, shape, and material property independent function of the liquid suspension concentration. In addition to these findings, we note that the ability to aerosolize nanomaterials down to 5 nm in size, preserving their size distribution, would enable a variety of analytical possibilities, including tandem ion mobility spectrometry[82,83] to examine vapor uptake or the evaporation of particles, IMS-inductively coupled plasma mass spectrometry[42] to infer size resolved chemical composition, and IMS coupled with aerosol particle mass analysis.[84] Though such techniques have been applied to particles in liquid suspensions previously, in nearly all

circumstances, aerosolization was accomplished with an electrospray, which as noted, has strict requirements on suspension salt concentration and electrical conductivity, limiting its use. The LN tested is capable of aerosolizing colloidal particles from hydrosols from a much wider range of conditions, and further, as it has higher throughput, leads to better counting statistics in gas phase measurements. We thus anticipate that LN based aerosolization will better facilitate characterization of sub 30 nm nanomaterials than electrospray based aerosolization.

Acknowledgements

This work was supported by US National Science Foundation Award CBET-1133285 (for the purchase of samples, reagents, and operation of the LN-IMS system) as well as United States Army Research Office Award MURI W911NF-12-0407 (to support S. Jeon). Electron microscopy was performed at the College of Science and Engineering Characterization Facility, University of Minnesota (UMN), which receives funding from the National Science Foundation through the UMN MRSEC under Award DMR-1420013.

References

1 C. Voisin, N. Del Fatti, D. Christofilos and F. Vallee, *J. Phys. Chem. B*, 2001, **105**, 2264–2280.
2 M. Nirmal and L. Brus, *Acc. Chem. Res.*, 1999, **32**, 407–414.
3 M. C. Daniel and D. Astruc, *Chem. Rev.*, 2004, **104**, 293–346.
4 D. Astruc, F. Lu and J. R. Aranzaes, *Angew. Chem., Int. Ed.*, 2005, **44**, 7852–7872.
5 A. Bootz, V. Vogel, D. Schubert and J. Kreuter, *Eur. J. Pharm. Biopharm.*, 2004, **57**, 369–375.
6 C. M. Hoo, N. Starostin, P. West and M. L. Mecartney, *J. Nanopart. Res.*, 2008, **10**, 89–96.
7 T. Ito, L. Sun, M. A. Bevan and R. M. Crooks, *Langmuir*, 2004, **20**, 6940–6945.
8 H. Jans, X. Liu, L. Austin, G. Maes and Q. Huo, *Anal. Chem.*, 2009, **81**, 9425–9432.
9 H. Hinterwirth, S. K. Wiedmer, M. Moilanen, A. Lehner, G. Allmaier, T. Waitz, W. Lindner and M. Lämmerhofer, *J. Sep. Sci.*, 2013, **36**, 2952–2961.
10 V. Filipe, A. Hawe and W. Jiskoot, *Pharm. Res.*, 2010, **27**, 796–810.
11 J. A. Gallego-Urrea, J. Tuoriniemi, T. Pallander and M. Hassellov, *Environ. Chem.*, 2010, **7**, 67–81.
12 H. Saveyn, B. De Baets, O. Thas, P. Hole, J. Smith and P. Van der Meeren, *J. Colloid Interface Sci.*, 2010, **352**, 593–600.
13 J. L. Axson, J. M. Creamean, A. L. Bondy, S. S. Capracotta, K. Y. Warner and A. P. Ault, *Aerosol Sci. Technol.*, 2014, **49**, 24–34.
14 J. L. Axson, D. I. Stark, A. L. Bondy, S. S. Capracotta, A. D. Maynard, M. A. Philbert, I. L. Bergin and A. P. Ault, *J. Phys. Chem. C*, 2015, **119**, 20632–20641.
15 J. P. Novak, C. Nickerson, S. Franzen and D. L. Feldheim, *Anal. Chem.*, 2001, **73**, 5758–5761.
16 M. Baalousha, B. Stolpe and J. R. Lead, *J. Chromatogr., A*, 2011, **1218**, 4078–4103.
17 J. Walter, K. Lohr, E. Karabudak, W. Reis, J. Mikhael, W. Peukert, W. Wohlleben and H. Colfen, *ACS Nano*, 2014, **8**, 8871–8886.
18 J. Walter, T. Thajudeen, S. Süβ, D. Segets and W. Peukert, *Nanoscale*, 2015, **7**, 6574–6587.
19 A. Dudkiewicz, S. Wagner, A. Lehner, Q. Chaudhry, S. Pietravalle, K. Tiede, A. B. A. Boxall, G. Allmaier, D. Tiede, R. Grombe, F. von der Kammer, T. Hofmann and K. Molhave, *Analyst*, 2015, **140**, 5257–5267.
20 J. Fernandez de la Mora, L. de Juan, T. Eichler and J. Rosell, *Trends Anal. Chem.*, 1998, **17**, 328–339.
21 M. R. Stolzenburg and P. H. Mcmurry, *Aerosol Sci. Technol.*, 1991, **14**, 48–65.
22 A. Wiedensohler, W. Birmili, A. Nowak, A. Sonntag, K. Weinhold, M. Merkel, B. Wehner, T. Tuch, S. Pfeifer, M. Fiebig, A. M. Fjaraa, E. Asmi, K. Sellegri, R. Depuy, H. Venzac, P. Villani, P. Laj, P. Aalto, J. A. Ogren, E. Swietlicki, P. Williams, P. Roldin, P. Quincey, C. Huglin, R. Fierz-Schmidhauser, M. Gysel, E. Weingartner, F. Riccobono, S. Santos, C. Gruning, K. Faloon, D. Beddows, R. M. Harrison, C. Monahan, S. G. Jennings, C. D. O'Dowd, A. Marinoni, H. G. Horn, L. Keck, J. Jiang, J. Scheckman, P. H. McMurry, Z. Deng, C. S. Zhao, M. Moerman, B. Henzing, G. de Leeuw, G. Loschau and S. Bastian, *Atmos. Meas. Tech.*, 2012, **5**, 657–685.
23 J. Y. Park, P. H. McMurry and K. Park, *Aerosol Sci. Technol.*, 2012, **46**, 354–360.
24 H. Fissan, S. Ristig, H. Kaminski, C. Asbach and M. Epple, *Anal. Methods*, 2014, **6**, 7324–7334.
25 S. L. Kaufman, *J. Aerosol Sci.*, 1998, **29**, 537–552.
26 L. de Juan and J. Fernandez de la Mora, *ACS Sym. Ser*, 1996, **622**, 20–41.
27 G. Bacher, W. W. Szymanski, S. L. Kaufman, P. Zollner, D. Blaas and G. Allmaier, *J. Mass. Spectrom.*, 2001, **36**, 1038–1052.
28 S. L. Kaufman, J. W. Skogen, F. D. Dorman, F. Zarrin and K. C. Lewis, *Anal. Chem.*, 1996, **68**, 1895–1904.
29 B. Han, I. W. Lenggoro, M. Choi and K. Okuyama, *Anal. Sci.*, 2003, **19**, 843–851.
30 I. W. Lenggoro, H. Widiyandari, C. J. Hogan, P. Biswas and K. Okuyama, *Anal. Chim. Acta*, 2007, **585**, 193–201.
31 I. W. Lenggoro, B. Xia, K. Okuyama and J. Fernandez de la Mora, *Langmuir*, 2002, **18**, 4584–4591.
32 S. Guha, X. Ma, M. J. Tarlov and M. R. Zachariah, *Anal. Chem.*, 2012, **84**, 6308–6311.
33 D. H. Tsai, F. W. DelRio, J. M. Pettibone, P. A. Lin, J. J. Tan, M. R. Zachariah and V. A. Hackley, *Langmuir*, 2013, **29**, 11267–11274.
34 D. H. Tsai, M. P. Shelton, F. W. DelRio, S. Elzey, S. Guha, M. R. Zachariah and V. A. Hackley, *Anal. Bioanal. Chem.*, 2012, **404**, 3015–3023.

35 L. F. Pease, D. H. Tsai, J. L. Hertz, R. A. Zangmeister, M. R. Zachariah and M. J. Tarlov, *Langmuir*, 2010, **26**, 11384–11390.
36 D. H. Tsai, F. W. DelRio, A. M. Keene, K. M. Tyner, R. I. MacCuspie, T. J. Cho, M. R. Zachariah and V. A. Hackley, *Langmuir*, 2011, **27**, 2464–2477.
37 D. H. Tsai, F. W. DelRio, R. I. MacCuspie, T. J. Cho, M. R. Zachariah and V. A. Hackley, *Langmuir*, 2010, **26**, 10325–10333.
38 L. F. Pease, D. H. Tsai, R. A. Zangmeister, M. R. Zachariah and M. J. Tarlov, *J. Phys. Chem. C*, 2007, **111**, 17155–17157.
39 D. H. Tsai, R. A. Zangmeister, L. F. Pease, M. J. Tarlov and M. R. Zachariah, *Langmuir*, 2008, **24**, 8483–8490.
40 M. Scalf, M. S. Westphall, J. Krause, S. L. Kaufman and L. M. Smith, *Science*, 1999, **283**, 194–197.
41 M. Scalf, M. S. Westphall and L. M. Smith, *Anal. Chem.*, 2000, **72**, 52–60.
42 S. Elzey, D.-H. Tsai, L. L. Yu, M. R. Winchester, M. E. Kelley and V. A. Hackley, *Anal. Bioanal. Chem.*, 2013, **405**, 2279–2288.
43 B. K. Ku, J. Fernandez de la Mora, D. A. Saucy and J. N. Alexander, *Anal. Chem.*, 2004, **76**, 814–822.
44 D. A. Saucy, S. Ude, I. W. Lenggoro and J. Fernandez de la Mora, *Anal. Chem.*, 2004, **76**, 1045–1053.
45 R. Müller, C. Laschober, W. W. Szymanski and G. Allmaier, *Macromolecules*, 2007, **40**, 5599–5605.
46 J. Fernandez de la Mora, *Anal. Chem.*, 2015, **87**, 3729–3735.
47 L. F. Pease, D. H. Tsai, K. A. Brorson, S. Guha, M. R. Zachariah and M. J. Tarlov, *Anal. Chem.*, 2011, **83**, 1753–1759.
48 G. Allmaier, C. Laschober and W. W. Szymariski, *J. Am. Soc. Mass Spectrom.*, 2008, **19**, 1062–1068.
49 G. Allmaier, A. Maisser, C. Laschober, P. Messner and W. W. Szymanski, *Trends Anal. Chem.*, 2011, **30**, 123–132.
50 C. J. Hogan, E. M. Kettleson, B. Ramaswami, D. R. Chen and P. Biswas, *Anal. Chem.*, 2006, **78**, 844–852.
51 J. J. Thomas, B. Bothner, J. Traina, W. H. Benner and G. Siuzdak, *J. Spectrosc.*, 2004, **18**, 31–36.
52 C. H. Wick and P. E. McCubbin, *Toxicol. Methods*, 1999, **9**, 245–252.
53 M. Havlik, M. Marchetti-Deschmann, G. Friedbacher, W. Winkler, P. Messner, L. Perez-Burgos, C. Tauer and G. Allmaier, *Anal. Chem.*, 2015, **87**, 8657–8664.
54 C. Laschober, J. Wruss, D. Blaas, W. W. Szymanski and G. Allmaier, *Anal. Chem.*, 2008, **80**, 2261–2264.
55 D. R. Chen and D. Y. H. Pui, *Aerosol Sci. Technol.*, 1997, **27**, 367–380.
56 D. R. Chen, D. Y. H. Pui and S. L. Kaufman, *J. Aerosol Sci.*, 1995, **26**, 963–977.
57 R. Gopalakrishnan, P. H. McMurry and C. J. Hogan, *J. Aerosol Sci.*, 2015, **82**, 24–39.
58 M. Li, R. You, G. W. Mulholland and M. R. Zachariah, *Aerosol Sci. Technol.*, 2013, **47**, 1101–1107.
59 P. Kallinger, G. Steiner and W. Szymanski, *J. Nanopart. Res.*, 2012, **14**, 1–8.
60 M. Shimada, B. W. Han, K. Okuyama and Y. Otani, *J. Chem. Eng. Jpn.*, 2002, **35**, 786–793.
61 A. Maisser, J. M. Thomas, C. Larriba-Andaluz, S. He and C. J. Hogan, *J. Aerosol Sci.*, 2015, **90**, 36–50.
62 R. Gopalakrishnan, M. R. Meredith, C. Larriba-Andaluz and C. J. Hogan, *J. Aerosol Sci.*, 2013, **63**, 126–145.
63 A. Wiedensohler, *J. Aerosol Sci.*, 1988, **19**, 387–389.
64 D. R. Chen, D. Y. H. Pui, D. Hummes, H. Fissan, F. R. Quant and G. J. Sem, *J. Aerosol Sci.*, 1998, **29**, 497–509.
65 S. C. Wang and R. C. Flagan, *Aerosol Sci. Technol.*, 1990, **13**, 230–240.
66 S. Jeon, T. Thajudeen and C. J. Hogan, *Powder Technol.*, 2015, **272**, 75–84.
67 C. Larriba, C. J. Hogan, M. Attoui, R. Borrajo, J. Fernandez-Garcia and J. Fernandez de la Mora, *Aerosol Sci. Technol.*, 2011, **45**, 453–467.
68 C. Zhang, T. Thajudeen, C. Larriba, T. E. Schwartzentruber and C. J. Hogan, *Aerosol Sci. Technol.*, 2012, **46**, 1065–1078.
69 P. G. Gormley and M. Kennedy, *Proc. R. Ir. Acad., Sect. A*, 1949, **52A**, 163–169.
70 R. Gopalakrishnan, P. H. McMurry and C. J. Hogan, *Aerosol Sci. Technol*, 2015, **49**, 1181–1194.
71 M. F. Bush, Z. Hall, K. Giles, J. Hoyes, C. V. Robinson and B. T. Ruotolo, *Anal. Chem.*, 2010, **82**, 9557–9565.
72 C. J. Hogan and J. Fernandez de la Mora, *J. Am. Soc. Mass Spectrom.*, 2011, **22**, 158–172.
73 A. Maiber, V. Premnath, A. Ghosh, T. A. Nguyen, M. Attoui and C. J. Hogan, *Phys. Chem. Chem. Phys.*, 2011, **13**, 21630–21641.
74 C. J. Hogan and P. Biswas, *J. Aerosol Sci.*, 2008, **39**, 432–440.
75 C. J. Hogan and P. Biswas, *J. Am. Soc. Mass Spectrom.*, 2008, **19**, 1098–1107.
76 K. C. Lewis, D. M. Dohmeier, J. W. Jorgenson, S. L. Kaufman, F. Zarrin and F. D. Dorman, *Anal. Chem.*, 1994, **66**, 2285–2292.
77 M. Li, S. Guha, R. A. Zangmeister, M. J. Tarlov and M. R. Zachariah, *Aerosol Sci. Technol.*, 2011, **45**, 849–860.
78 C. Larriba-Andaluz, J. Fernandez-Garcia, C. J. Hogan and D. E. Clemmer, *Phys. Chem. Chem. Phys.*, 2015, **17**, 15019–15029.
79 J. H. Kim, G. W. Mulholland, S. R. Kukuck and D. Y. H. Pui, *J. Res. Natl. Inst. Stand. Technol.*, 2005, **110**, 31–54.
80 H. Jung, K. Han, G. W. Mulholland, D. Y. H. Pui and J. H. Kim, *J. Aerosol Sci.*, 2013, **65**, 42–48.
81 B. Giechaskiel, X. Wang, H. G. Horn, J. Spielvogel, C. Gerhart, J. Southgate, L. Jing, M. Kasper, Y. Drossinos and A. Krasenbrink, *Aerosol Sci. Technol.*, 2009, **43**, 1164–1173.
82 H. Ouyang, S. He, C. Larriba-Andaluz and C. J. Hogan, *J. Phys. Chem. A*, 2015, **119**, 2026–2036.
83 D. J. Rader and P. H. McMurry, *J. Aerosol Sci.*, 1986, **17**, 771–787.
84 N. Tajima, H. Sakurai, N. Fukushima and K. Ehara, *Aerosol Sci. Technol.*, 2013, **47**, 1152–1162.